Available online at www.sciencedirect.com
ScienceDirect
Icarus 196 (2008) 216–224
ICARUS
www.elsevier.com/locate/icarus

Resurfacing of Titan by ammonia-water cryomagma

Giuseppe Mitri [a,*], Adam P. Showman [b], Jonathan I. Lunine [b,c], Rosaly M.C. Lopes [a]

[a] *Jet Propulsion Laboratory, California Institute of Technology, 4800 Oak Grove Drive, Pasadena, CA 91109, USA*
[b] *Department of Planetary Sciences and Lunar and Planetary Laboratory, University of Arizona, Tucson, AZ, USA*
[c] *Istituto di Fisica dello Spazio Interplanetario INAF-IFSI, Roma, Italy*

Received 8 August 2005; revised 13 February 2008

Available online 29 March 2008

Abstract

The Cassini Titan Radar Mapper observed on Titan several large features interpreted as cryovolcanic during the October 26, 2004 pass at high northern latitudes [Lopes, R.M.C., and 43 colleagues, 2007. Icarus 186, 395–412]. To date, models of ammonia-water resurfacing have not been tied to specific events or evolutionary stages of Titan. We propose a model of cryovolcanism that involves cracking at the base of the ice shell and formation of ammonia-water pockets in the ice. As these ammonia-water pockets undergo partial freezing in the cold ice shell, the ammonia concentration in the pockets increases, decreasing the negative buoyancy of the ammonia–water mixture. If the ice shell is contaminated by silicates delivered in impacts, the liquid–solid density difference would be even less. While the liquid cannot easily become buoyant relative to the surrounding ice, these concentrated ammonia-water pockets are sufficiently close to the neutral buoyancy point that large-scale tectonic stress patterns (tides, non-synchronous rotation, satellite volume changes, solid state convection, or subsurface pressure gradients associated with topography) would enable the ammonia to erupt effusively onto the surface. Rather than suggesting steady-state volcanism over the history of the Solar System, we favor a scenario where the cryovolcanic features could have been associated with episodic (potentially late) geological activity.

Keywords: Titan; Saturn; Volcanism; Satellites, surfaces; Interiors; Ices; Geophysics

1. Introduction

Remote sensing observations yield evidence for cryovolcanism on Titan (Fig. 1; see also Elachi et al., 2005; Sotin et al., 2005; Tomasko et al., 2005; Lopes et al., 2007), and evolutionary models support (but do not require) the presence of an ammonia-water subsurface ocean on Titan (e.g., Grasset et al., 2000; Tobie et al., 2005; Mitri and Showman, 2008a). The impetus for invoking ammonia as a constituent in an internal ocean and cryovolcanic magma comes from two factors. First, ammonia-water liquid has a lower freezing temperature than pure liquid water, enabling cryovolcanism under the low-temperature conditions prevalent in the outer Solar System. Second, pure water is negatively buoyant with respect to pure water ice, which discourages eruption from the subsurface ocean to the surface (e.g., Showman et al., 2004). In contrast, the addition of ammonia to the water decreases its density, hence lessening this problem of negative buoyancy. The condition of close neutral buoyancy of an ammonia–water mixture at peritectic temperature has led to the hypothesis that resurfacing might occur by ammonia-water cryomagma (Lewis, 1972; Croft et al., 1988; Kargel et al., 1991; Lorenz, 1996; Lopes et al., 2007). The prediction by accretion models of the presence of ammonia within Titan (e.g., Mousis et al., 2002) supports this hypothesis. Ammonia hydrate, trapped in ice during the accretion period of Titan, could be released in a liquid layer after the formation of Titan's silicate core (Lunine and Stevenson, 1987; Mousis et al., 2002). Recently, circumstantial evidence from mass spectrometric measurements indicates the past and possibly present-day existence of ammonia within Titan (Niemann et al., 2005; Waite et al., 2005).

However, the peritectic ammonia-water liquid with a composition near that of pure ammonia dihydrate ($NH_3 \cdot 2H_2O$) has a density (946 kg m^{-3}) that is close to neutral buoyancy with

* Corresponding author.
E-mail address: giuseppe.mitri@jpl.nasa.gov (G. Mitri).

0019-1035/$ – see front matter
doi:10.1016/j.icarus.2008.02.024

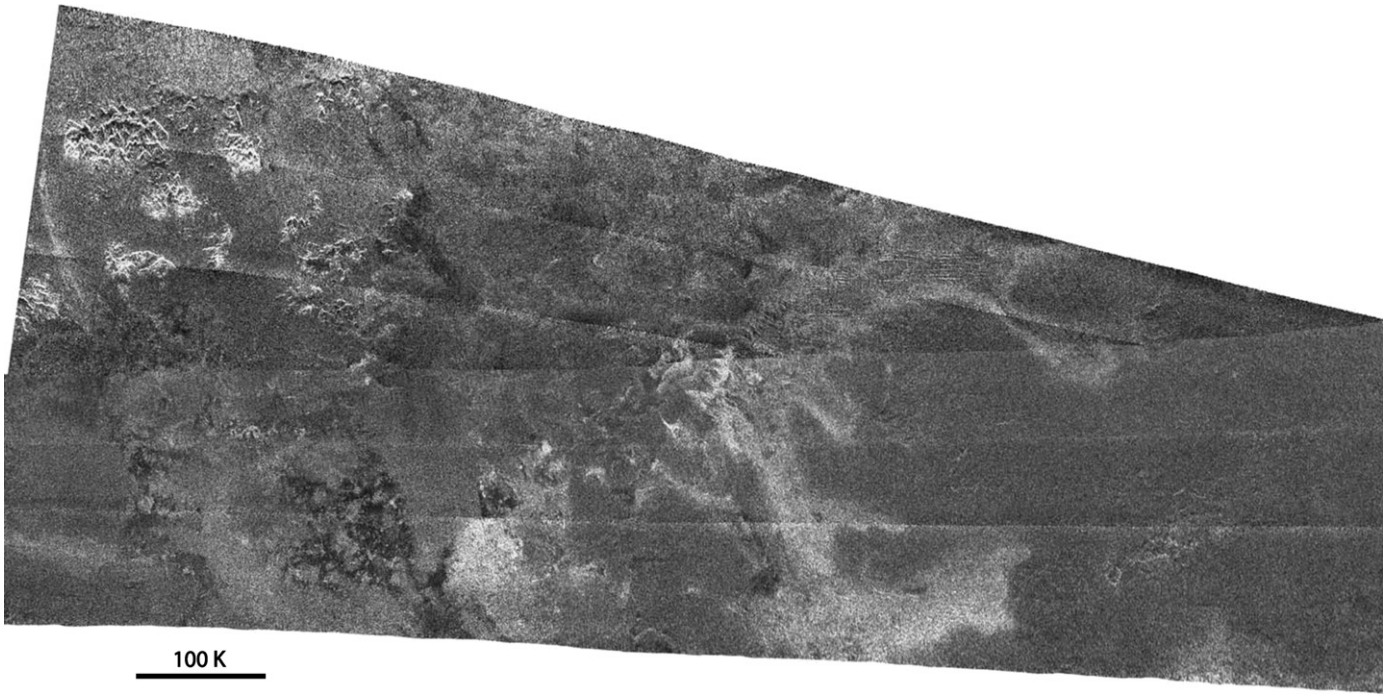

Fig. 1. Large flow called Winia Fluctus imaged by the Titan Radar Mapper using the SAR mode during the fly-by on October 26, 2004. The area is around 90,000 km^2. The image is centered at about 45° N, 30° W. The radar illumination is from the south. Note that the southern edges of the flow are brighter, consistent with the structure being raised above the relatively featureless darker background. This is one of several flows imaged by SAR interpreted to be cryovolcanic in origin (see Lopes et al., 2007).

respect to the water ice (920 kg m^{-3}). A marginally positive buoyant mixture might allow effusive eruptions from a subsurface ocean (Croft et al., 1988). If the subsurface ocean were positively buoyant, all the ammonia would have been erupted very early in Titan's history. Either the surface would be full of ancient cryovolcanic features, or erosion would have erased all of these. Contrary to this scenario, Cassini–Huygens has so far observed neither a global abundance nor a complete dearth of cryovolcanic features. Further, an ancient cryovolcanic epoch cannot explain the relative youth of Titan's surface (0.2–1 Gyr; Lorenz et al., 2007). Crucial to invoking ammonia-water resurfacing as the source of the apparently recent geological activity is not how to make ammonia-water volcanism work (because the near neutral buoyancy of the ammonia–water mixture encourages an explanation), but rather how to prevent eruption from occurring so easily that cryovolcanic activity is over early on (D.J. Stevenson, pers. commun., 2006). The questions naturally arise: What are the physical conditions by which ammonia-water could have erupted from Titan's interior? Can cryovolcanism be related to a specific episode or chapter of Titan's thermal evolution?

Several mechanisms have been proposed for cryovolcanic eruptions on icy satellites: gas exsolution following depressurization in fluid-filled fractures that propagate upward from the base of the ice shell (Crawford and Stevenson, 1988); resurfacing by tidal pumping of water from an internal ocean (Greenberg et al., 1998); explosive eruptions of sprays (Fagents et al., 2000); pressurization of liquid chambers in an ice-I shell (Fagents, 2003; Showman et al., 2004); and resurfacing driven by pressurization of the entire ocean during satellite volume changes (most relevant to bodies substantially smaller than Titan; Manga and Wang, 2007). Lorenz (1996) proposed a mechanism based on cryomagma transport to the surface through cracks in Titan's ice-I shell. Showman et al. (2004) proposed for Ganymede that tidal heating partially melts the shallow ice shell (between 5 and 10 km from the surface). They have shown that surface topography (for example graben) produces pressure gradients within the ice shell that might pump water from the interior of the ice shell to the surface. Fortes et al. (2007) proposed a resurfacing model on Titan based on the assumption that large amounts of sulfur leached into the internal ocean; we do not pursue this model further because the leaching has yet to be quantitatively calculated, and radiometric data from Cassini (Paganelli et al., 2007) are not consistent with large amounts of ammonium-sulfate compounds on the surface.

Here we test the hypothesis that ammonia-water can promote resurfacing and we propose a model of cryovolcanism on Titan.

2. Model

2.1. Internal structure

Formation and thermal models indicate that Titan should be at least partially differentiated with a multi-layer internal structure divided into a rocky interior, a high-pressure ice (HP) layer, an ammonia-water subsurface ocean, and an outer ice-I shell (e.g., Grasset et al., 2000; Tobie et al., 2006; Mitri and Showman, 2008a; Rappaport et al., 2008). Fig. 2 illustrates the nominal Titan's internal structure adopted (see Mitri and Showman, 2008a).

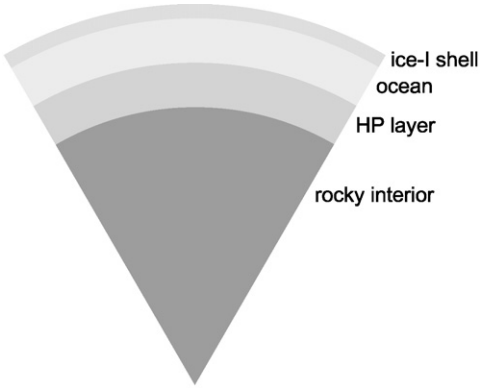

Fig. 2. Model of Titan's internal structure. The multilayer model of the interior is divided into a rocky interior, an ice high pressure (HP) layer, an ammonia-water ocean, and an ice-I shell (see Mitri and Showman, 2008a).

2.2. Ice and ammonia–water mixture densities

In order to evaluate whether ammonia–water mixture is negatively/positively buoyant with respect to the water ice, we determine the dependence of these densities over a lithospheric pressure range of 0–0.1 GPa. The density of the ice depends on the pressure and at high pressure exceeds the value 917 kg m^{-3} that is measured under normal laboratory conditions. We determine the density of the ice as

$$\rho_{\rm ice} = \rho_0 \cdot \left[\frac{K_0'}{K_0} P + 1\right]^{1/K_0'}, \tag{1}$$

where ρ_0 is the reference density at normal laboratory conditions, P is the pressure, K_0' (5.5) and K_0 (9.2 GPa) are, respectively, the pressure derivative of the bulk modulus and the bulk modulus (e.g., Tobie et al., 2006). The density of the ammonia–water liquid mixture is determined following Croft et al. (1988) with $K_0' = 5.0$ and $K_0 = 2.5$ GPa.

2.3. Bottom crevasses

Bottom crevasses—that is, cracks ascending from the base of an ice shell—have been observed within terrestrial ice shelves (van der Veen, 1998a, 1998b). Here, we investigate whether cracks at the base of the ice-I shell can occur on Titan, and we will study their role for cryovolcanic activity. Following the terminology of glaciology, we will call bottom crevasses those cracks that are at the base of the ice-I shell.

We apply the linear elastic fracture mechanics (LEFM) to crack formation in the ice shell. A discussion of the applicability of LEFM to describe crevasse formation on glaciers can be found in van der Veen (1998a, 1998b). The intensity fracture toughness K_I takes into account the stress concentration near the crack tip. We write the intensity fracture toughness for a field of closely spaced crevasses as

$$K_I = \sqrt{\pi h}(\sigma_n - \Delta\rho g h), \tag{2}$$

where h is the height of the bottom crevasse above the base of the ice shell, σ_n is the tensional stress, $\Delta\rho$ is the difference of density between the ocean and the ice, and g is the gravity (1.35 m s^{-2}). The height h of an isolated crevasse includes a correction factor $\pi/2$, to take into account the stress concentration at the crack tip (Weertman, 1973; van der Veen, 1998b). Rist et al. (1996) measured that the fracture toughness for ice samples from the Ross Ice Shelf (Antarctica) range between ~0.1–0.4 MPa m$^{1/2}$.

We will compare the LEFM theory results with those obtained with the zero stress model. The total stress $\sigma_n(z)$ that acts on a bottom crevasse in the ice shell is

$$\sigma_n(z) = -\Delta\rho g z + \sigma, \tag{3}$$

where z is the vertical coordinate and $z = 0$ at the base of the ice shell, and σ is the stress. However, the maximum height h of a bottom crevasse is given by the condition that $z = h$ for $\sigma_n(z) = 0$ (Weertman, 1980; van der Veen, 1998b).

Tidal stresses act on the ice shell, and might create and maintain bottom crevasses. The driving frequency ω of the tidal stress in Titan's ice shell is the orbital frequency (4.56×10^{-6} s^{-1}). The tidal distortion of Titan relative to a spherical shape is given by (see Greenberg and Geissler, 2002)

$$d = h_2\left(\frac{3}{2}\cos^2\theta - \frac{1}{2}\right)\left[R_T \frac{M_S}{M_T}\left(\frac{R_T}{a}\right)^3\right], \tag{4}$$

where h_2 is the Love number ($h_2 \sim 1.2$; Sohl et al., 2003), M_S is Saturn's mass (5.68×10^{26} kg), M_T is Titan's mass (1.346×10^{23} kg), R_T is Titan's radius (2575 km), a is the orbital semi-major axis (1.2208×10^6 km), and θ is the angle between the line-of-sight to Saturn and the local vertical at any point on Titan's surface. The amplitude of the tidal flexing of the ice shell is given by $\xi \sim 3ed$ (Greenberg and Geissler, 2002), where e is the orbital eccentricity ($e = 0.0292$). The maximum amplitude of the ice shell tidal-flexing strain is determined to order-of-magnitude as $\varepsilon_0 \sim \xi/R_T$ (Showman and Han, 2004; Mitri and Showman, 2005). We find that the maximum tidal distortion is ~120 m, the maximum amplitude of the tidal flexing of the ice shell is ~11 m, and the tidal-flexing strain is $\sim 4 \times 10^{-6}$.

The tidal stresses as a function of the ice-shell temperature are determined solving the flow law of the water ice in the form of a Maxwellian viscoelastic body

$$\dot{\varepsilon}(t) = \frac{\dot{\sigma}(t)}{\mu} + \frac{\sigma(t)}{\eta(T)}, \tag{5}$$

where $\dot{\varepsilon}(t)$ is the strain rate, $\sigma(t)$ is the stress, dot denotes the derivation in time t, μ is the rigidity of the ice (4×10^9 Pa), and $\eta(T)$ is the temperature (T) dependent viscosity of the ice. The Newtonian viscosity of the ice is given by (see discussion in Mitri and Showman, 2008b)

$$\eta = \eta_0 \exp\left[A\left(\frac{T_{\rm ref}}{T} - 1\right)\right], \tag{6}$$

where η_0 is the ice viscosity at a temperature of 273 K ($10^{13} \leqslant \eta_0 \leqslant 10^{15}$ Pa s), the constant $A = 26$, corresponding to an activation energy of 60 kJ mol^{-1} and $T_{\rm ref} = 273$ K is a reference temperature.

2.4. Percolation in the ice shell

The densities of water and ammonia-water liquid both exceed that of water ice. In the absence of other factors, the liquid percolates downward. In order to compare the percolation velocity ($v_{\rm perc}$) with convective motion velocity in the ice, we determine $v_{\rm perc}$ of liquid in a solid matrix as

$$v_{\rm perc} = \frac{\kappa^* \Delta\rho g}{\eta_l} \frac{(1-\phi)}{\phi}, \tag{7}$$

where κ^* is the permeability, $\Delta\rho$ is the difference of density between the liquid and the ice, g is the gravity, η_l is the viscosity of the liquid, and ϕ is the liquid fraction in the matrix.

For a small liquid fraction in the ice, the permeability of the ice is (Stevenson and Scott, 1991)

$$\kappa^* \sim \kappa_0^* d_{\rm gs}^2 \phi^2, \tag{8}$$

where $d_{\rm gs}$ is the grain size and κ_0^* is $\sim 10^{-3}$ (e.g., Showman et al., 2004).

Combining Eqs. (7) and (8), the percolation velocity is

$$v_{\rm perc} = \frac{\kappa_0 d_{\rm gs}^2 \Delta\rho g \phi (1-\phi)}{\eta_l}. \tag{9}$$

The viscosity (η_l) of a liquid pocket in the ice shell ranges from 0.002 Pa s (pure water) to 10 Pa s (ammonia-water peritectic) (Kargel et al., 1991). The viscosity can be higher if the mixture contains other components such as methanol. The viscosity of ammonia-water–methanol at its low-pressure peritectic point is 10^4 Pa s (Kargel et al., 1991).

2.5. Topographic resurfacing

Showman et al. (2004) showed that subsurface stress fields produced by surface topography can pump negatively buoyant liquid within the ice shell to the surface, thereby promoting resurfacing. The model was developed for pore-space liquid water within an interconnected network. The topographic pressure gradients are the same in microscopic pores or macroscopic pockets. Therefore we can apply this model to Titan in the case of macroscopic pockets. Under the action of a stress field, liquid flow in a matrix is driven by an ahydrostatic pressure gradient given by $-\nabla(\eta\nabla\vec{v})$, where η and $\vec{v}$ are the shear viscosity and vector velocity of the matrix, respectively. The analytical solution derived by Showman et al. (2004) gives the stress fields produced by topography. The Showman et al. model assumes that the liquid fraction within the matrix is constant, and the surface topography is sinusoidal $\delta = \delta_0(\cos 2\pi x/\lambda)$, where δ_0 is the topography height, x is the horizontal distance, and λ is the wavelength. Under these assumptions, the pressure gradients within the ice shell are

$$-\nabla P = \rho g \delta_0 \frac{2\pi}{\lambda} e^{\frac{2\pi}{\lambda}z} \left[\sin\left(\frac{2\pi}{\lambda}x\right)\hat{x} - \cos\left(\frac{2\pi}{\lambda}z\right)\hat{z} \right], \tag{10}$$

where ρ is the density, z is the height and it is equal zero at the surface, $\hat{x}$ and $\hat{z}$ are the horizontal and the vertical unit vectors, respectively. The net pressure gradient that drives the liquid through the matrix is the sum of the pressure gradient $-\nabla P$ and the negative buoyancy of the liquid $-\Delta\rho g\hat{z}$, where $\Delta\rho$ is the difference of density between the ice and the liquid. See Showman et al. (2004) for further discussion.

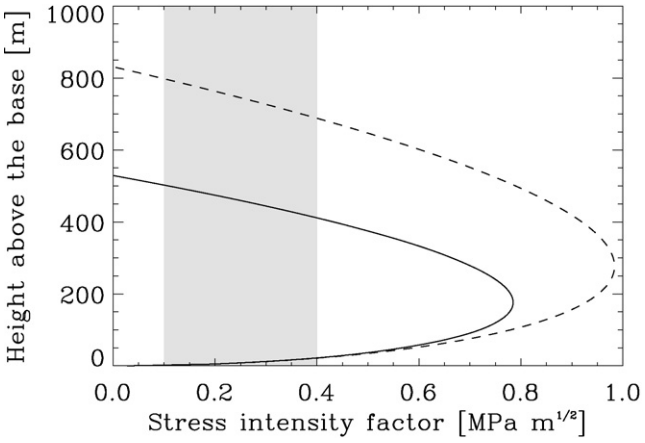

Fig. 3. Stress intensity factor as a function of the height above the ice shell. The tensile stress is 5×10^4 Pa and difference in density between the ocean fluid and the ice is 70 kg m^{-3}. The solid line shows the crack height in a field of closely spaced crevasses; the dashed line shows the crack height above the base of the ice shell for an isolated crevasse. The gray area corresponds to fracture toughness for ice that range between 0.1 and 0.4 MPa m$^{1/2}$.

3. Results and discussion

3.1. Bottom crevasses

Analogously to terrestrial ice shelves, bottom crevasses can form at the base of the ice-I shell of Titan. Defects within an elastic body present as preexisting small cracks can propagate as large fractures if stresses are applied. The bottom crevasses have a high penetration depth because ocean water fills the cracks, and therefore the pressure of the water on the crevasse walls counters the hydrostatic pressure of the ice that tends to close the fractures. Fig. 3 shows the stress intensity factor as a function of the height above the base of the ice shell for a constant tensile stress 5×10^4 Pa and a difference in density between the fluid and the ice of 70 kg m^{-3}. The solid line shows the crack height in a field of closely spaced crevasses; the dashed line shows the crack height for an isolated crevasse where stress concentration occurs at the tip of the crack. Consider an isolated bottom crevasse in the ice shell (solid line). For a constant tensile stress with depth, the stress intensity factor close to the base of the ice shell depends on the square root of the crack height. Near the base of the ice shell the hydrostatic pressure of the water and the lithostatic pressure are roughly equal. Therefore, when the crack grows the stress intensity factor increases. In a deeper crack filled with water, the lithostatic pressure is higher than the hydrostatic pressure of the water. Therefore the net longitudinal stress decreases and consequently the stress intensity factor decreases. The gray area of Fig. 3 corresponds to a fracture toughness for ice that ranges between 0.1–0.4 MPa m$^{1/2}$. A crack propagates whether or not the stress intensity fracture K_I is larger than the fracture toughness $K_{\rm Icr}$. We see in Fig. 3 that $K_I = K_{\rm Icr}$ has two solutions:

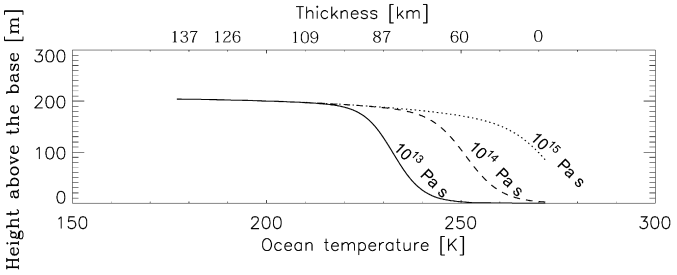

Fig. 4. Height above the base of the ice shell of bottom crevasses as a function of the basal temperature and thickness of the ice shell. The initial ammonia concentration of the ocean is 5%, the ice density is 917 kg m^{-3}, and the viscosity of the ice at the melting temperature is 10^{13} Pa s (solid line), 10^{14} Pa s (dashed line), and 10^{15} Pa s (dotted line).

the first solution is for a crack height close to the base of the ice shell, and the second solution is for a much deeper crack in the ice. The first solution is unstable (van der Veen, 1998a, 1998b): a small perturbation can force the crack to close completely or open progressively until it reaches the second solution. However, the second solution is stable and corresponds to the maximum extent of penetration of the crack (van der Veen, 1998b). In our example, the stable solution corresponds to an extent of penetration of the crack of ∼500 m. We note that the simple zero stress model predicts that the extent of penetration is 530 m (corresponding to the stress intensity factor equal to zero in Fig. 3).

Crevasse formation requires that small cracks are present at the base of the ice shell. The tensile strength of ice as measured in small laboratory-samples is of the order of 10^6 Pa. However, field experiments on the Ross Ice Shelf in Antarctica indicate that the ice shelf has much smaller failure strengths of $\sim 10^5$ Pa (Kehle, 1964). Furthermore, the existence of cycloidal ridges (Hoppa et al., 1999) and other tidal stress-generated tectonic features on Europa (e.g., Greenberg et al., 1998) suggest that Europa's ice shell has failure strengths comparable to the $\sim 10^5$ Pa tidal stress. These arguments lend weight to the possibility that Titan's ice shell is likewise weak and able to fracture under the influence of tidal stresses. Weertman (1980) and van der Veen (1998b) have shown that, in terrestrial ice, small cracks can be formed through brine entrapment during ice refreezing and by etching (caused by liquid water) of grain boundaries in the ice. These processes can also form small cracks in Titan's ice shell. Potentially, non-synchronous rotation of the ice shell and/or volume changes of Titan (that can occur during melting/refreezing of the ice-I shell) could lead to sufficient stresses for bottom crevasse formation. Tidal stresses can marginally produce small cracks in the ice-I shell, but if preexisting fractures are present, the tidal stress will maintain the fractures over time. Fig. 4 shows the extent of penetration of a bottom crevasse maintained by tidal stress. The tidal flexing strain is 4×10^{-6}, and the tidal stress is computed solving the flow law of the water ice in form of a Maxwellian viscoelastic material. The model is for a uniform ice density of 917 kg m^{-3}, the reference viscosity of the ice at melting temperature is 10^{13} Pa s (solid line), 10^{14} Pa s (dashed line), and 10^{15} Pa s (dotted line), and the initial ammonia concentration in the liquid layer is 5%. Fig. 4 shows that the extent of penetration of a bottom crevasse maintained by tidal stress can be of the order of hundreds of meters.

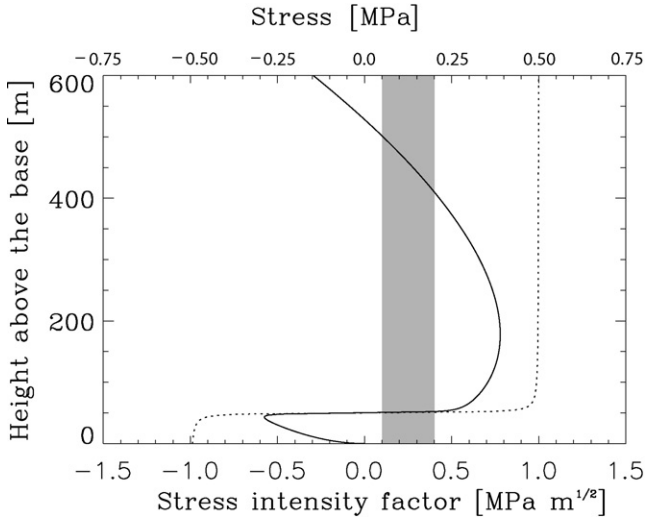

Fig. 5. Extent of penetration of a bottom crevasse above the base of the ice shell as a function of the stress intensity factor (solid line) for a compressive stress at the base and a tensile stress in the middle of the crack (dotted line). The gray area corresponds to fracture toughness for ice that range between 0.1–0.4 MPa m$^{1/2}$.

Refrozen bottom crevasses are common features in terrestrial ice shelves. In a freezing crevasse the ice grows laterally into the crack, implying that the crack cannot trap liquid in the ice during its crystallization (Petrich et al., 2007). On other hand, we expect that the trapped ocean fluid in an open crack during the tidal flexing of the ice shell is almost all expelled before a new tidal cycle occurs. To trap liquids in the ice, the base of the ice shell must be under compression and at the same time the middle part of the crack must be unstressed or under extension. Fig. 5 shows the height above the base of the ice shell as a function of the stress intensity factor (solid line) for a compressive stress at the base and a tensile stress in the middle of the crack (dotted line). A suitable process is the rapid refreezing of the ice shell base such that the interior of a deep crack does not itself become frozen. Convection can aid this process by allowing rapid changes in ice thickness (Mitri and Showman, 2008a). Tobie et al. (2005) have shown that the orbital evolution of Titan gives a significant variation in heat flux on timescales of order of 10^8 yr. A faster and larger variation in thickness of the ice shell is expected if the onset of convection occurs in the ice. In this case changes in the thickness of the ice shell of several tens of kilometers in a timescale of $\sim 10^7$ yr are expected (Mitri and Showman, 2008a).

3.2. State of the ammonia-water liquid in the ice shell

If the ice-I shell contains liquid ammonia-water pockets that partially freeze, then the ammonia concentration can approach the eutectic within these pockets. Freezing of ammonia-water pockets in the ice shell might allow the liquid trapped in the ice shell to become close to neutrally buoyant even when the ocean itself is not buoyant.

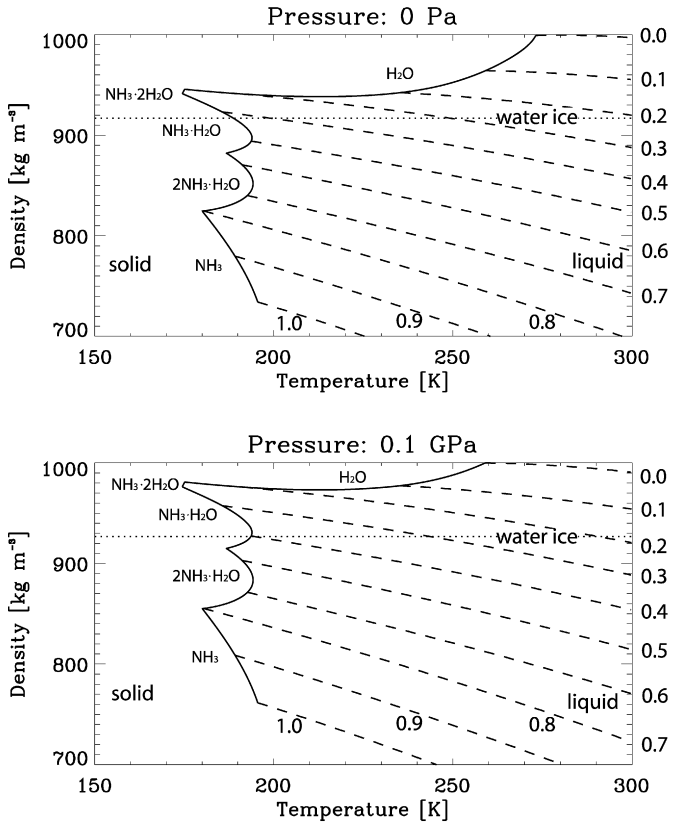

Fig. 6. Relationship between the density, temperature and composition for the ammonia–water system for a litostathic pressure of 0 and 0.1 GPa. The solid curves give the liquidus and where the ammonia–water mixture crystallizes into H_2O, $NH_3{\cdot}2H_2O$, $NH_3{\cdot}H_2O$, $2NH_3{\cdot}H_2O$, and NH_3. The dashed lines give the density of liquid ammonia-water as a function of temperature for a fixed ammonia concentration (0–1.0 range). The dotted lines show the water ice density.

Fig. 6 shows the relationship between the density, temperature and composition for the ammonia–water system for litostathic pressures of 0 GPa and 0.1 GPa. The solid curves give the liquidus and indicate where the ammonia–water mixture crystallizes into H_2O, $NH_3{\cdot}2H_2O$, $NH_3{\cdot}H_2O$, $2NH_3{\cdot}H_2O$, and NH_3. The dashed lines give the density of liquid ammonia-water as a function of temperature for a fixed ammonia concentration ($0 < x < 1.0$). The dotted line gives the water ice density. An ammonia-water pocket in thermal equilibrium with the surrounding ice freezes following the liquidus (solid line). In case of thermal equilibrium with the surrounding ice, the ammonia-water pocket temperature might rise somewhat above the eutectic temperature so that the pocket is close to neutral buoyancy.

However, an ammonia-water pocket in the ice shell at the eutectic temperature is not quite buoyant. For pure water ice the difference in density is ∼20–30 kg m^{-3}. The ice density is further enhanced by addition of mixed rock-ice impactors over geologic time. This acts to increase the buoyancy of ammonia-water pockets. (The very uppermost tens or even hundreds of meters of this layer might be porous in places, but this will not affect the overall densification of the shell due to the exogenous addition of silicates.) Following a procedure similar to that in Showman et al. (2004), we estimate the increase in density using crater density relations between the impactor mass, transient cavity diameter, and final diameter in Zahnle et al. (2003). For example, assuming an apparent diameter of an impact crater of 80 km, an impactor density of 600 kg m^{-3} consistent with the density of Comet Shoemaker–Levy 9 (dominated by the porosity of the comet), an intrinsic density of the impactor material of 1500–2000 kg m^{-3}, and an impact velocity range 3–15 km s^{-1} (Artemieva and Lunine, 2005), we determine that the enhancement in density within the ejecta removed from the crater is 1–3%, in agreement with an earlier investigation for Ganymede (Showman et al., 2004). The mass delivered is dominated by the largest impactors. Over the history of Titan, the overlap of impact ejecta blankets produces a surface layer ∼10–20 km thick of dirty ice with a density enhancement of a few percent. Even considering the surface layer of dirty ice, it is difficult for an ammonia-water pocket in equilibrium with the surrounding ice to reach positive buoyancy and promote resurfacing.

3.3. Resurfacing

While the liquid density in ammonia-water pockets cannot easily become buoyant relative to the surrounding ice, the concentrated ammonia-water pockets are sufficiently close to neutrally buoyant that large-scale tectonic stress patterns would enable the ammonia to erupt effusively onto the surface, at least episodically. Stresses associated with tides, non-synchronous rotation, satellite volume changes, and solid-state convection in the ice may all promote an environment where near-neutrally buoyant ammonia-water residing in subsurface pockets can be delivered effusively onto the surface at localized times and places.

Eruptions might occur by a variety of different tectonic settings. Thermal convection in ice might play an important role. Liquid pockets of ammonia-water can be transported from the base of the ice shell to the base of the stagnant lid in a convective-overturn time scale (10^4–10^5 years; Mitri and Showman, 2005, 2008a). A convective ice shell has a drop of temperature in the convective sublayer of the order of 10–20 K (Mitri and Showman, 2005). The temperature of the convective region is so warm that ammonia-water pockets, which have a peritectic temperature of 177 K, cannot completely freeze. Thus, the cryomagma will be preserved in a liquid state during convective transport to the stagnant lid.

Percolation can potentially drain ammonia-water liquid from a macroscopic subsurface liquid pocket. Fig. 7 shows the percolation velocity of an ammonia–water mixture depending on the viscosity of the liquid and ice grain size (1 mm in solid lines, 10 mm in dotted lines). The difference in density between the liquid and the ice is 20 kg m^{-3}. The model is for two melt fractions: $\phi = 0.001$ and $\phi = 0.01$. At depths greater than a few kilometers, lithostatic pressures are sufficient to close empty pore spaces, so one expects low porosities at depth. Values of $\phi = 0.001$–0.01 are appropriate for systems experiencing partial melting, where melting at grain boundaries produces an interconnected network of microscopic passages through which liquid can flow (e.g., Turcotte and Schubert, 2002, pp. 402;

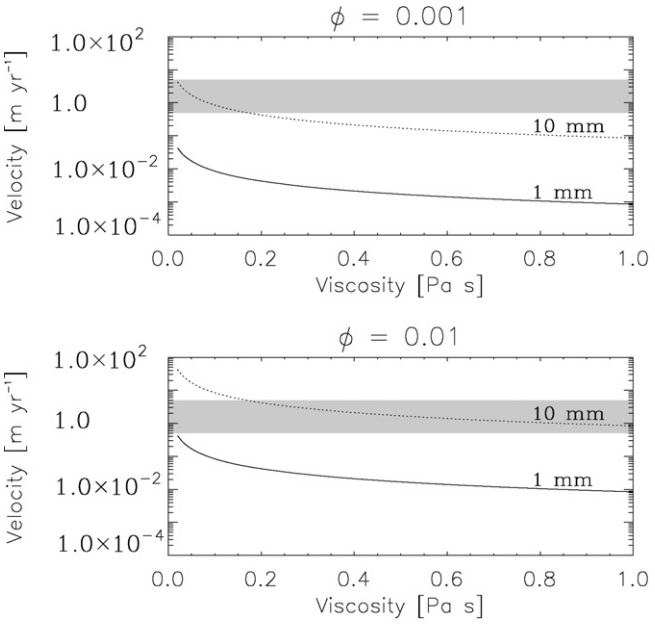

Fig. 7. Percolation velocity through the ice shell of an ammonia water mixture versus the viscosity, and the ice grain size (1 mm in solid lines, 10 mm in dotted lines). The difference in density between the liquid and the ice is 20 kg m^{-3}. The plots are for two melt fractions: $\phi = 0.001$ and $\phi = 0.01$. Grey areas show the convective velocity of the ice (0.5–5 m yr^{-1} range).

Showman et al., 2004). In our case, however, ammonia-water liquid with a low melting temperature is percolating through relatively pure ice with a higher melting temperature, so the percolation is not accompanied by melting or the associated production of melt channels. Thus, we envision that melt fractions $\phi = 0.001$–0.01 are upper limits for the present situation. Fig. 7 compares the percolation velocity with a convective velocity of the ice that ranges from 0.5 to 5 m yr^{-1} (in gray area). The figure shows that in general the convective velocity is greater than the percolation velocity, and therefore ammonia-water pockets can be transported upward by convective motions in the ice.

Stress gradients associated with topography ($-\nabla P$) could contribute to resurfacing, as has been suggested for Ganymede (Showman et al., 2004). Showman et al. presented an analytic solution for the subsurface flow of pore-space liquid under the assumption that the melt fraction is constant. Adopting this model, Figs. 8 and 9 show the pressure gradients (panel B) and the net pressure gradients (panel C) for a sinusoidal topography with two different amplitudes. The pressure gradient fields show the direction of the ice flow (panel B). The net pressure gradient ($-\nabla P - \Delta\rho g\hat{z}$) drives the liquid to flow within a matrix of the ice. In absence of topography the liquid percolates downward in the direction of the pressure gradients $-\Delta\rho g\hat{z}$. However, pressure gradients associated with topography could be sufficiently high to produce upward flows underneath topographic lows. The arrows of panel C in Figs. 8 and 9 indicate the direction of liquid flows through a matrix of the ice. Assuming a density $\rho = 920$ kg m^{-3}, a difference of density $\Delta\rho = 26$ kg m^{-3} between the liquid and the ice, and a topographic amplitude $\delta_0 = 0.5$ km (Fig. 8) and 1 km (Fig. 9) and a wavelength $\lambda = 30$ km, the liquid can percolate upward in

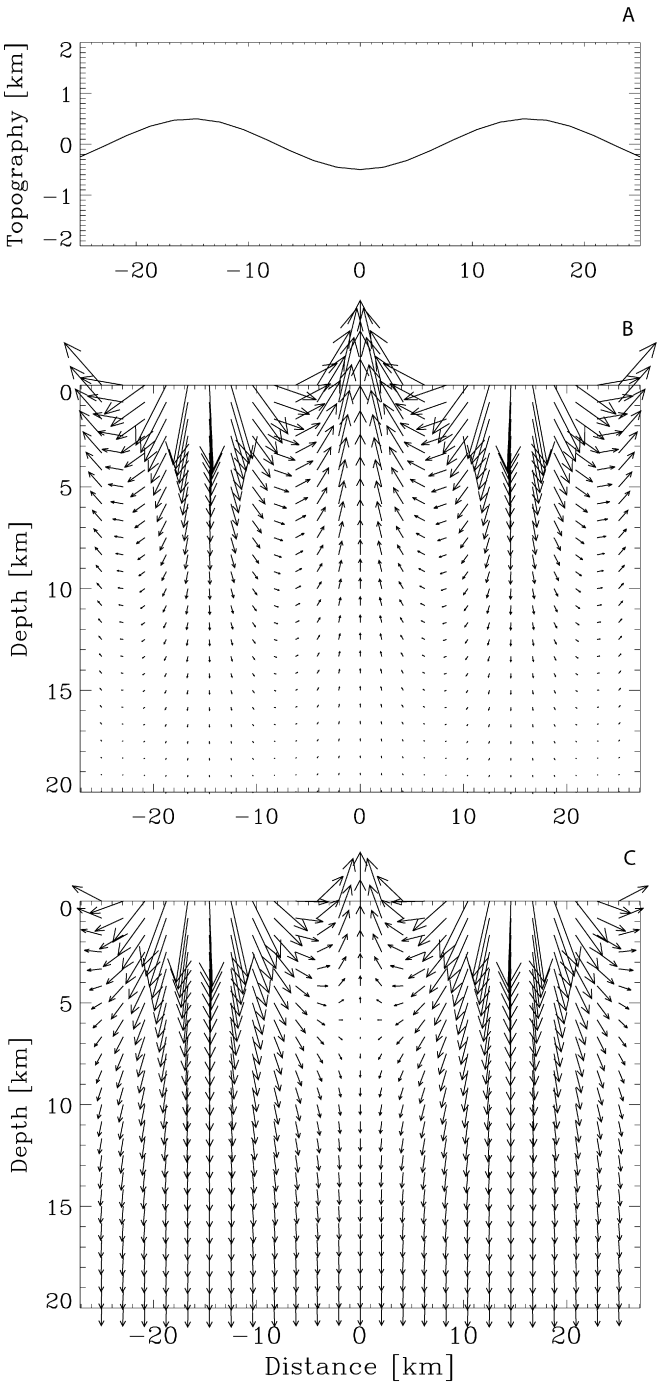

Fig. 8. Pressure gradients (panel B), and the net pressure gradients affecting pore-space liquid water (panel C) for a sinusoidal topography (panel A). The density is $\rho = 920$ kg m^{-3}, the difference of density is $\Delta\rho = 26$ kg m^{-3}, the wavelength is $\lambda = 30$ km, and the topographic amplitude is $\delta_0 = 0.5$ km. The maxima (larger arrows in the plots) of the pressure gradients (B) and net pressure gradients (C) are 130 and 95 Pa m^{-1}, respectively. Based on the model of Showman et al. (2004).

the area corresponding at low topography. The maxima (larger arrows in the plots) of the pressure gradients (panel B) and net pressure gradients (panel C) are 130 and 95 Pa m^{-1} for $\delta_0 = 0.5$ km, and 260 and 225 Pa m^{-1} for $\delta_0 = 1.0$ km, respectively.

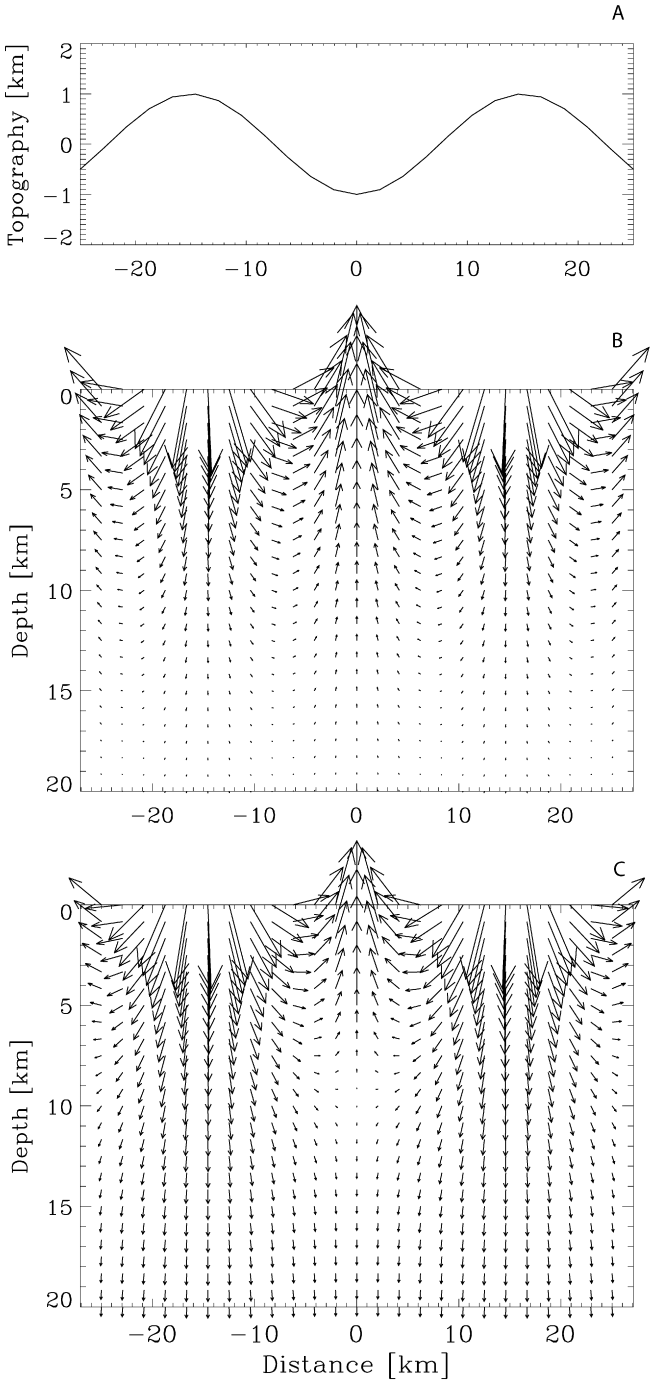

Fig. 9. Pressure gradients (panel B), and the net pressure gradients affecting pore-space liquid water (panel C) for sinusoidal topography (panel A). The density is $\rho = 920\ \mathrm{kg\,m^{-3}}$, the difference of density is $\Delta\rho = 26\ \mathrm{kg\,m^{-3}}$, the wavelength is $\lambda = 30$ km, and the topographic amplitude is $\delta_0 = 1.0$ km. The maxima (larger arrows in the plots) of the pressure gradients (B) and net pressure gradients (C) are 260 and 225 $\mathrm{Pa\,m^{-1}}$, respectively. Based on the model of Showman et al. (2004).

Exsolution of soluble gases near the surface would also promote eruption of liquid onto the surface. Methane clathrate is stable in the ice shell in the absence of destabilizing thermal perturbations and/or pressure variations. However, methane outgassing because of methane clathrate dissociation in the ice shell by cryovolcanism activity can produce the present methane abundance in the atmosphere.

4. Conclusions

Although cryovolcanism by ammonia-water has been proposed as a resurfacing process on Titan, few models have specifically dealt with the problem of how to transport ammonia-water liquid onto the surface. We proposed a model of cryovolcanism that involve cracking at the base of the ice shell and formation of ammonia-water pockets in the ice. While the ammonia-water pockets cannot easily become neutral buoyant and promote effusive eruptions, large scale tectonics stress (due to tides, non-synchronous rotation, satellite volume changes, and/or topography) may all promote resurfacing at localized times and spaces. Thermal convection in the ice-I shell can play an important role in ensuring recent cryovolcanism activity on Titan.

Ammonia-water pockets trapped in the ice shell provides a possible mechanism for explaining episodic cryovolcanism on Titan. Our model has several advantages over more simplistic ones. Because of the relative inefficiency of trapping liquid in the shell and transporting it to the surface, our mechanism makes volcanism a "marginal" process. In this way we can explain why Titan did not lose all its ammonia into cryovolcanic flows early in Solar System history as would happen were ammonia-water liquid to be positively buoyant, hence making cryovolcanism too "easy." At the same time, in our mechanism allows cryovolcanism to be an important process on regional scales: ammonia should be present at the surface and hence detectable so long as it is not buried by subsequent sedimentation of organic aerosols. Finally, because we posit that the cryovolcanic liquid comes from localized pockets rather than directly from the ocean, our scenario also allows the ocean to remain dilute in ammonia, hence much denser than the overlying ice and mechanically stable over the history of the Solar System.

Acknowledgments

We thank two anonymous reviewers, whose comments improved the manuscript. This project was supported by the NASA PG&G program through Grant NNG04GI46G to A.P.S., and a contract to J.L. from the Cassini project. G.M. was supported by an appointment to the NASA Postdoctoral Program at the Jet Propulsion Laboratory. Parts of this work were carried out at the Jet Propulsion Laboratory, California Institute of Technology under a contract from NASA, and (J.L.) at the Institute for the Physics of Interplanetary Space (IFSI), Rome, Italy.

References

Artemieva, N., Lunine, J.I., 2005. Impact cratering on Titan. II. Global melt, escaping ejecta, and aqueous alteration of surface organics. Icarus 175, 522–533.

Crawford, G.D., Stevenson, D.J., 1988. Gas-driven water volcanism in the resurfacing of Europa. Icarus 73, 66–79.

Croft, S.K., Lunine, J.I., Kargel, J., 1988. Equation of state of ammonia-water liquid—Derivation and planetological applications. Icarus 73, 279–293.
Elachi, C., and 34 colleagues, 2005. Cassini Radar views the Surface of Titan. Science 308, 970–974.
Fagents, S.A., 2003. Considerations for effusive cryovolcanism on Europa: The post-Galileo perspective. J. Geophys. Res. 108, doi:10.1029/2003JE002128. 13-1.
Fagents, S.A., Greeley, R., Sullivan, R.J., Pappalardo, R.T., Prockter, L.M., and The Galileo SSI Team, 2000. Cryomagmatic mechanisms for the formation of Rhadamanthys Linea, Triple Band Margins, and other low-albedo features on Europa. Icarus 144, 54–88.
Fortes, A.D., Grindrod, P.M., Trickett, S.K., Vočadlo, L., 2007. Ammonium sulfate on Titan: Possible origin and role in cryovolcanism. Icarus 188, 139–153.
Grasset, O., Sotin, C., Deschamps, F., 2000. On the internal structure and dynamics of Titan. Planet. Space Sci. 48, 617–636.
Greenberg, R., Geissler, P., 2002. Europa's dynamic icy crust. Meteorit. Planet. Sci. 37, 1685–1710.
Greenberg, R., Geissler, P., Hoppa, G., Tufts, B.R., Durda, D.D., Pappalardo, R., Head, J.W., Greeley, R., Sullivan, R., Carr, M.H., 1998. Tectonic processes on Europa: Tidal stresses, mechanical response, and visible features. Icarus 135, 64–78.
Hoppa, G.V., Tufts, B.R., Greenberg, R., Geissler, P.E., 1999. Formation of cycloidal features on Europa. Science 285, 1899–1902.
Kargel, J.S., Croft, S.K., Lunine, J.I., Lewis, J.S., 1991. Rheological properties of ammonia-water liquids and crystal–liquid slurries—Planetological applications. Icarus 89, 93–112.
Kehle, R.O., 1964. Deformation of the Ross Ice Shelf, Antarctica. Geol. Soc. Am. Bull. 75, 259–286.
Lewis, J.S., 1972. Low temperature condensation from the solar nebula. Icarus 16, 241.
Lopes, R.M.C., and 43 colleagues, 2007. Cryovolcanic features on Titan's surface as revealed by the Cassini Titan Radar Mapper. Icarus 186, 395–412.
Lorenz, R.D., 1996. Pillow lava on Titan: Expectations and constraints on cryovolcanic processes. Planet. Space Sci. 44, 1021–1028.
Lorenz, R.D., and 11 colleagues, 2007. Titan's young surface: Initial impact crater survey by Cassini Radar and model comparison. Geophys. Res. Lett. 34, doi:10.1029/2006GL028971. 7204.
Lunine, J.I., Stevenson, D.J., 1987. Clathrate and ammonia hydrates at high pressure—Application to the origin of methane on Titan. Icarus 70, 61–77.
Manga, M., Wang, C.Y., 2007. Pressurized oceans and the eruption of liquid water on Europa and Enceladus. Geophys. Res. Lett. 34, 7202.
Mitri, G., Showman, A.P., 2005. Convective–conductive transitions and sensitivity of a convecting ice shell to perturbations in heat flux and tidal-heating rate: Implications for Europa. Icarus 177, 447–460.
Mitri, G., Showman, A.P., 2008a. Thermal convection in ice-I shells of Titan and Enceladus. Icarus 193, 387–396.
Mitri, G., Showman, A.P., 2008b. A model for the temperature-dependence of tidal dissipation in convective plumes on icy satellites: Implications for Europa and Enceladus. Icarus, doi:10.1016/j.icarus.2008.01.010, in press.
Mousis, O., Gautier, D., Coustenis, A., 2002. The D/H ratio in methane in Titan: Origin and history. Icarus 159, 156–165.
Niemann, H.B., and 17 colleagues, 2005. The abundances of constituents of Titan's atmosphere from the GCMS instrument on the Huygens probe. Nature 438, 779–784.
Paganelli, F., and 14 colleagues, 2007. Titan's surface from Cassini Radar SAR and high resolution radiometry data of the first five flybys. Icarus 191, 211–222.
Petrich, C., Langhorne, P.J., Haskell, T.G., 2007. Formation and structure of refrozen cracks in land-fast first-year sea ice. J. Geophys. Res. 112, doi:10.1029/2006JC003466. C04006.
Rappaport, N.J., Iess, L., Wahr, J., Lunine, J.I., Armstrong, J.W., Asmar, W., Tortora, P., Di Benedetto, M., Racioppa, P., 2008. Can Cassini detect a subsurface ocean in Titan from gravity measurements? Icarus 194, 711–720.
Rist, M.A., Sammonds, P.R., Murrel, S.A.F., Meredith, P.G., Oerter, H., Doake, C.S.M., 1996. Experimental fracture and mechanical properties of Antarctic ice: Preliminary results. Ann. Glaciol. 23, 284–292.
Showman, A.P., Han, L., 2004. Numerical simulations of convection in Europa's ice shell: Implications for surface features. J. Geophys. Res. 109 (E1), doi:10.1029/2003JE002103. E01010.
Showman, A.P., Mosqueira, I., Head, J.W., 2004. On the resurfacing of Ganymede by liquid-water volcanism. Icarus 172, 625–640.
Sohl, F., Hussmann, H., Schwentker, B., Spohn, T., Lorenz, R.D., 2003. Interior structure models and tidal Love numbers of Titan. J. Geophys. Res. 108. 4-1.
Sotin, C., VIMS Cassini team, 2005. Release of volatiles from a possible cryovolcano from near-infrared imaging of Titan. Nature 435, 786–789.
Stevenson, D.J., Scott, D.R., 1991. Mechanics of fluid–rock systems. Annu. Rev. Fluid Mech. 23, 305–339.
Tobie, G., Grasset, O., Lunine, J.I., Mocquet, A., Sotin, C., 2005. Titan's internal structure inferred from a coupled thermal-orbital model. Icarus 175, 496–502.
Tobie, G., Lunine, J.I., Sotin, C., 2006. Episodic outgassing as the origin of atmospheric methane on Titan. Nature 440, 61–64.
Tomasko, M.G., and 39 colleagues, 2005. Rain, winds and haze during the Huygens Probe's descent to Titan's surface. Nature 438, 765–778.
Turcotte, D.L., Schubert, G., 2002. Geodynamics, second ed. Cambridge Univ. Press, Cambridge.
van der Veen, C.J., 1998a. Fracture mechanics approach to penetration of surface crevasses on glaciers. Cold Reg. Sci. Technol. 27, 31–47.
van der Veen, C.J., 1998b. Fracture mechanics approach to penetration of bottom crevasses on glaciers. Cold Reg. Sci. Technol. 27, 213–223.
Waite, H., and 21 colleagues, 2005. Ion-neutral mass spectrometer results from the first flyby of Titan. Science 308, 982–986.
Weertman, J., 1973. Can a water-filled crevasse reach the bottom surface of a glacier? IAHS Publ. 95, 139–145.
Weertman, J., 1980. Bottom crevasses. J. Glaciol. 25, 185–188.
Zahnle, K., Schenk, P., Levison, H., Dones, L., 2003. Cratering rates in the outer Solar System. Icarus 163, 263–289.